Journal of Hydrology 673 (2026) 135336

Contents lists available at ScienceDirect

Journal of Hydrology

journal homepage: www.elsevier.com/locate/jhydrol

Research papers

A new approach for groundwater fluxes assessment in alluvial aquifers using active-DTS with a Brillouin-based sensor

Jordan Labbe [a,*], Maxime Romanet [b], Hélène Celle [a], Maxime Zerbib [b], Kien Phan Huy [b,c], Alexandre Matic [b], Victor Klaba [a], Gilles Mailhot [d], Jean-Charles Beugnot [b]

[a] Université Marie et Louis Pasteur, Chrono-Environnement UMR CNRS 6249, Besançon, France
[b] Université Marie et Louis Pasteur, Institut FEMTO-ST UMR CNRS 6174, Besançon, France
[c] SUPMICROTECH-ENSMM, 16 Rue de l'Epitaphe, Besançon, France
[d] CNRS, SIGMA Clermont, Institut de Chimie de Clermont-Ferrand, Université Clermont Auvergne, F-63000 Clermont-Ferrand, France

ARTICLE INFO

This manuscript was handled by Renato Morbidelli, Editor-in-Chief, with the assistance of Bertil Nlend Associate Editor

Keywords:
Brillouin
Active-DTS
Fiber optic
Groundwater flux
Alluvial aquifer

ABSTRACT

Fiber optic distributed temperature sensing has become a widely used approach to estimate groundwater fluxes in various hydrogeological contexts. Raman-based sensors are the most commonly adopted DTS units but they rely on calibration baths that may be challenging to maintain for experiments extending over several days. In this paper, a novel method using a Brillouin-based sensor (DITEST) is proposed. This approach relies on the linear relationship between the Brillouin Frequency Shift and the fiber temperature which is not affected by optical losses. The proposed methodology was tested at the experimental site of Port-Douvot where an Electrical Resistivity Tomography profile and a core sample were conducted to assess vertical and lateral heterogeneities. These investigations have identified that the alluvial deposits extend to an average thickness of 10 m with a top layer of clayey sands (~5 m) overlying a second layer of coarse gravel and pebbles (~5 m). Point Dilution Tests were carried out to investigate the range of possible groundwater fluxes q, the results of which have revealed fluxes ranging from 1.2×10^{-5} to 8.2×10^{-7} m/s. Brillouin active-DTS measurements were conducted with a spatial resolution of 1 m, a sampling interval of 0.25 m and a temperature sensitivity of 0.2°C. The vertical variations of horizontal groundwater fluxes q are consistent with subsurface heterogeneities. Estimated fluxes spanned a shorter interval than Point Dilution Tests, between 1.0×10^{-7} to 7.0×10^{-7} m/s, but remain plausible. The fact that frequency measurements are absolute and do not require any field calibration makes Brillouin sensing an attractive tool for long-term monitoring.

1. Introduction

The assessment of aquifer hydrodynamic properties has traditionally relied on what may be referred to as 'conventional' methods such as pumping tests (Butler, 1990; Kollet and Zlotnik, 2003; Dashti et al., 2022) and tracer experiments (Derouane and Dassargues, 1998; Dann et al., 2008). These approaches are essential for quantifying groundwater flow potential or solute transport and are therefore commonly implemented in groundwater resource management frameworks. Although these tests are efficient and easily replicable, they only provide one value of hydraulic conductivity K or groundwater flux q, after one experiment. Moreover, conventional methods may be insufficient to resolve the spatial variability of aquifer properties resulting from lateral and vertical heterogeneities.

More advanced approaches now increasingly rely on thermal-based techniques. The main objective of these methods is to use temperature a natural tracer of groundwater movement. This may be achieved by carrying out ambient temperature profiles (Anderson, 2005) for instance, temperatures time-series (Saphores et al., 2024), thermal tracer tests (Klepikova et al., 2016), passive (Furlanetto et al., 2024) and active distributed temperature sensing (A-DTS) using fiber optics (Selker and Selker, 2018; Banks et al., 2022; Sai Louie et al., 2023), the examples of applications are numerous.

Fiber Optic-DTS methods are more sophisticated and now widely used as they provide temperature data at a higher spatial and temporal resolution than conventional techniques. They rely on the installation of a fiber-optic cable (FO cable) in a borehole or buried in the ground at varying depths (Shanafield et al., 2018). In each of these experiments, a

* Corresponding author.
E-mail address: jordan.labbe@univ-fcomte.fr (J. Labbe).

https://doi.org/10.1016/j.jhydrol.2026.135336
Received 24 October 2025; Received in revised form 12 March 2026; Accepted 16 March 2026
Available online 20 March 2026

DTS unit is used to both send a laser pulse into the optical fiber and detect reflected (or backscattered) signals (Simon, 2020). Three types of backscattered signals can be detected and analyzed to assess hydrological processes: Raman, Brillouin and Rayleigh (Selker et al., 2006; Chai and Luo, 2019). In the scope of hydrogeological applications, Raman appears to be the most commonly used (Tyler et al., 2009; Coleman et al., 2015; Hausner et al., 2016; Simon et al., 2022), as it offers a good compromise between its temperature sensitivity, accuracy and spatial resolution (Ukil et al., 2012). The Rayleigh scattering measurement is distinguished by its high accuracy and spatial resolution (Schenato, 2017) but requires a careful calibration. Rayleigh-based sensors can only measure a temperature variation from a specific reference (Palmieri et al., 2022). Rayleigh-based DTS methods are not usually employed in the field because the measurement is too sensitive to ambient noise and requires a controlled environment to obtain clean measurements (Boyd et al., 2011; Joshua et al., 2022).

Brillouin is the third type of backscattering light that can be detected and analyzed in an optical fiber. In Raman backscatter measurements, the fiber temperature is inferred from the ratio of Stokes and anti-Stokes intensities while in the case of Brillouin, the temperature dependence appears through shifts in the Brillouin frequency (Bao et al., 1993). DTS Brillouin-based techniques are commonly used for the monitoring and surveillance of civil infrastructures such as bridges, railways, pipelines or photovoltaic installations (Ravet et al., 2006; Galindez-Jamioy and López-Higuera, 2012; Guzowski et al., 2025; Wang et al., 2025). Indeed, the Brillouin signal is sensitive to both strain and temperature (Thevenaz et al., 1998) which makes it a valuable tool for civil monitoring. However, it has been rarely used in environmental sciences. One of the first "hydrological applications" was the measurement of the Geneva lake bed temperature (Nikles et al., 1996; Selker et al., 2006). Brillouin backscattering detected in an optical fiber is indeed affected by the surrounding temperature. If the latter increases, the intensity and frequency of Brillouin scattering also increases (Romanet, 2024). Moreover, Romanet et al., (2023) have demonstrated that it is possible to detect a hotspot at 100 km on a standard telecommunication fiber cable using Brillouin Optical Time Domain Reflectometry (BOTDR). Thus, it is already a valuable tool in civil engineering and could be a powerful approach for the monitoring of environmental parameters as well. The use of Brillouin offers indeed a considerable advantage over Raman and Rayleigh, based on a direct measurement of the absolute frequency along the FO cable, we are able to estimate a temperature without using any field-calibration (unlike Raman). Along a FO cable, there may be optical losses particularly due to splices which can affect the signal intensity but not its frequency. Bearing all these factors in mind, we therefore believe that the Brillouin-based DTS is a promising method for hydrogeological applications and it deserves to be tested in the field.

The assessment of groundwater fluxes remains a significant challenge across a wide range of hydrogeological contexts and spatial scales (Hermans et al., 2023). Conventional methods often rely on simplifying assumptions and models (i.e. homogeneous and isotropic medium) which are usually limiting for a detailed characterization of aquifer properties. The deployment of a FO cable provides substantial advantages as it enables spatially continuous data acquisition, offering enhanced environmental characterization across the field of interest.

In this study, we explored the use of a Brillouin sensor to measure groundwater fluxes in an alluvial aquifer, which to our knowledge has never been attempted before. This approach was tested in a DTS setup deployed on the experimental site of Port-Douvot (Besançon, France). The study site is implanted in an alluvial aquifer which is first characterized by conventional techniques (Electrical Resistivity Tomography, extraction of a core sample, estimation of groundwater fluxes by conducting Point Dilution Tests) and then characterized by a more advanced approach (FO-DTS). The purpose of our work is to demonstrate that we can use a Brillouin-based sensor to measure groundwater fluxes in natural flow conditions and correlate them with the lateral and vertical heterogeneities of the medium.

2. Materials and methods

2.1. Study site settings

The experimental site of Port-Douvot (H + National Observation Service, AUVERWATCH site) is located in eastern France, near Besançon, on the right bank of the Doubs River (Fig. 1a). The river flows from NE to SW. The alluvial floodplain on which the site is located is 160 m wide and 10 m thick and consists of sandy-gravelly alluvial deposits overlying a marly bedrock.

The site is equipped with nine boreholes (Fig. 1b) including eight piezometers (PZ1 to PZ8) and one well (W01). All boreholes are fully penetrating the alluvial aquifer except for PZ6/PZ4/PZ3 which are completed with screen intervals at different depths. PZ1 to PZ8 have an inner fully screened PVC casing (Ø52 mm). A continuous *BruSens LLK-BTSE 85°C* fiber optic (FO) cable was installed along the PZ7-PZ8-W01 line (Fig. 1b). Five "fiber holes" F1 to F5 (Fig. 1b) were drilled to insert the FO cable directly into the alluvial deposits. A temporary steel casing was employed during fiber installation to support the drilled hole and inhibit premature collapse (Fig. 1c). Once the substratum was reached, the fiber was placed vertically, the steel casing was removed and we left F1-F5 to fill in naturally. In each fiber hole, the FO cable was ballasted with steel weights and curved into a loop at the bottom of each of the five holes (Fig. 1d). This prevents the fibers from touching or intermingling which could interfere with temperature measurements. Splices were made to join all the fibers into a single continuous line (Fig. 2).

Groundwater flow is driven by the hydraulic gradient imposed by the Doubs River (located at 40 m from W01) which is 0.10% on average. In comparison, the mean hydraulic gradient between PZ6 and W01 (following the groundwater flow direction) is 0.16%. A pumping test carried out on W01 showed that the hydraulic conductivity K is 5×10^{-2} m/s which is consistent with the presence of coarse gravels and pebbles (Domenico and Schwartz, 1998).

2.2. Field data collection

2.2.1. Conventional methods to characterize subsurface heterogeneities: core sample and Electrical Resistivity Tomography

Various conventional methods were initially applied to characterize the lateral and vertical heterogeneities of the alluvial deposits. Vertical heterogeneities were identified by the extraction between PZ3 and W01 (Fig. 1b) of a continuous 9.94 m long core sample. High-resolution pictures of all the segments of the core were taken with a Multi-Sensor Core Logger *Geotek Ltd.* (Sedilog) at the Chrono-Environnement laboratory. Lateral heterogeneities were evidenced by a 2D ERT survey that was undertaken to create a cross-section of the subsurface resistivity to obtain an overview of the shallow alluvial aquifer. ERT data were collected with a Syscal R1+ (*Iris Instruments*) with 36 electrodes spaced 1.5 m apart, in a Wenner-Schlumberger electrode configuration. The 2D ERT panel was 54 m long and was oriented NE-SW, parallel to the Doubs River (Fig. 1b). The apparent resistivity data were inverted with RES2DINV software using the least-squares inversion method (Loke and Barker, 1996).

2.2.2. A conventional solute tracer test to characterize groundwater fluxes: Point Dilution Tests

Five Point Dilution Tests (PDTs) were conducted to estimate the Darcy flux q (m/s) of the aquifer using the following boreholes: PZ1, PZ5, PZ6, PZ3 and PZ7 (Fig. 1b). The PDT is a single-well technique that involves injecting a mass M (g) of tracer into an observation borehole and monitor at a constant timestep the evolution of electrical conductivity EC (µS/cm) over time t (s) in the same injection borehole (Williams et al., 2006; Piccinini et al., 2016). A CTD-Diver sensor (*SDEC©*) was configured to measure EC every 60 s in each tested borehole (EC measurement accuracy is ± 1%). The CTD-Diver is installed prior to

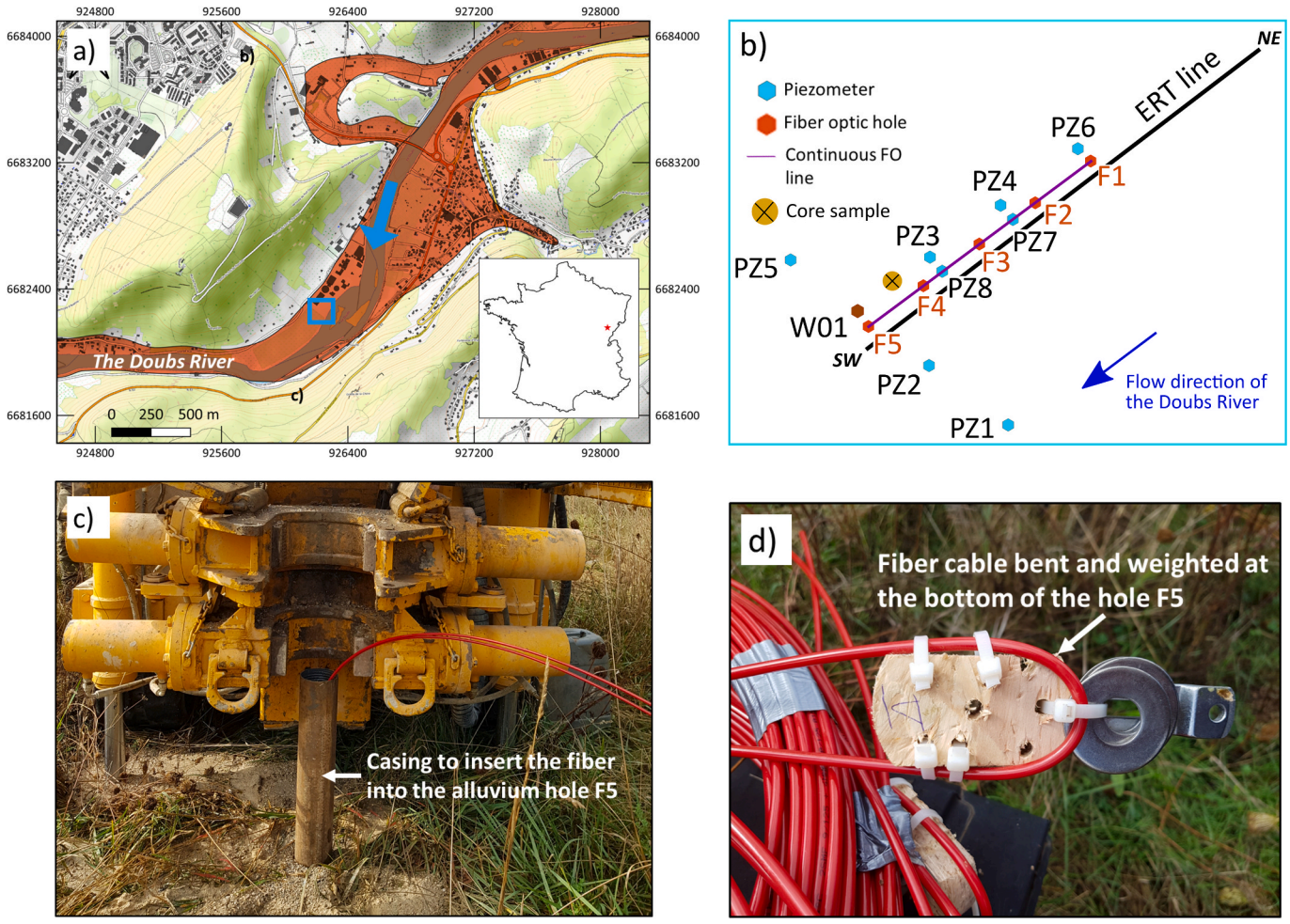

Fig. 1. (a) Location of the experimental site of Port-Douvot in the Doubs River floodplain (brown), the blue square refers to Fig. 1b, (b) location of the boreholes and the fiber optic line, (c) picture showing how the FO cable was inserted directly into the ground, d) picture showing how the FO cable was set and ballasted with weights at the bottom of the all FO holes. (For interpretation of the references to colour in this figure legend, the reader is referred to the web version of this article.)

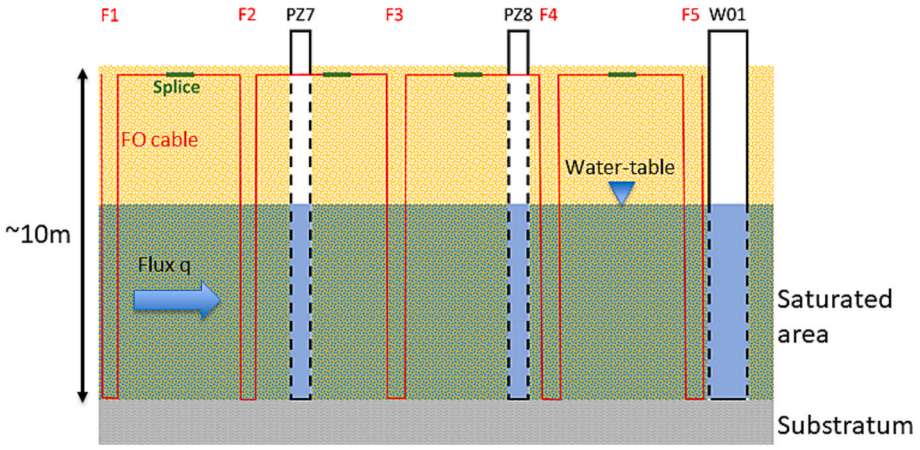

Fig. 2. Cross-section of the PZ7-PZ8-W01 borehole line showing the positioning of the continuous FO cable in the alluvial aquifer.

injection to measure the background *EC* ($EC_{background}$) caused by all dissolved ionic substances naturally present in groundwater. $EC_{background}$ was used to correct the observed *EC* values due to injection (Palmer, 1993). Before injection and during the PDT, the borehole water was continuously recirculated to ensure the tracer homogenization throughout the water column (Jamin and Brouyère, 2018).

A calibration curve was determined to convert the measured *EC* into equivalent concentrations *C* (Lamontagne et al., 2002). For each PDT, 2000 g of NaCl were dissolved in a container with local groundwater (= volume V_1). In the tested borehole before injection, the CTD-Diver monitors $EC_{background}$ (the volume of water in the borehole is V_2), this phase corresponds to $C = 0$ g/l of injected tracer. When the saline

solution is injected, the CTD-Diver measures $EC_{background} + \Delta_{EC}$ (i.e. the increase in EC due to injection). The initial concentration C_0 (g/l) thus corresponds to the mass of tracer M diluted in $V_1 + V_2$ which leads to an increase in EC (Δ_{EC}). C_0 is then equivalent to the maximum value of EC observed (EC_{max}) at the beginning of the PDT. For the calibration curve, we therefore obtain a linear relationship relating the evolution of C_t to EC measured by the CTD-Diver: $C_t = a \times EC\ (CTD\text{-}Diver) + b$.

The interpretation is based on the following assumption: the decline of C_t in the borehole is proportional to both the apparent velocity V_a (m/s) in the borehole section, i.e. the groundwater flow occurring only in the borehole (Piccinini et al., 2016) and to the Darcy flux q (m/s) in the aquifer. If the tracer dilution is only caused by the groundwater flux and considering steady flow conditions, the tracer concentration C decreases over time t following Eq. (1), (Freeze and Cherry, 1979).

$$\frac{dC}{dt} = -\frac{A\nu_a C}{W} \tag{1}$$

With ν_a the apparent velocity (m/s), A the cross-sectional area (m^2) perpendicular to the groundwater flow direction and the dilution volume W (l) ($W = V_1 + V_2$). If the tracer dilution is indeed only due to groundwater fluxes, then the LN of the ratio C/C_0 exhibits a linear relationship with time and ν_a can be estimated using Eq. (2).

$$\nu_a = m\left(\frac{\pi r}{2}\right) \tag{2}$$

where m is the slope of the curve and r the radius (m) of the tested well. The Darcy flux q (m/s) is then estimated by accounting for the flow field distortion α ($V_a = \alpha \times q$) which may be caused by the presence of the piezometer (Drost et al., 1968; Piccinini et al., 2016). PDTs of PZ6 and PZ3 were conducted during low-flow conditions whereas those for PZ1, PZ5 and PZ7 are more representative of medium to high-flow conditions, if based on the Doubs River discharge (Table 1).

2.2.3. A more advanced method for estimating groundwater fluxes: Brillouin-based DTS

2.2.3.1. Principle of the active-DTS method using optical fiber. The purpose of the Active-DTS method is to use temperature as a natural tracer of groundwater fluxes. This is made possible because the temperature of the medium (saturated or not) in which the fiber is installed affects the backscattered signals, Raman is modified in intensity and Brillouin shifts in frequency (Romanet et al., 2026). The 'Active' method consists in increasing the temperature of the fiber in order to obtain a stable and clean thermal response which can be achieved by heating the fiber with a heatpulse (HPS) system. In our case study, we will therefore enhance the frequency shift of the Brillouin signal.

2.2.3.2. Field setup on the experimental site. The DITEST (developed by *Omnisens*) is the Brillouin-based sensor that is used to interrogate and collect the frequency data along the FO cable. The measurement parameters are determined by the design of the sensor and in the present case by the pump pulse. The Brillouin interrogator sends an incident light at telecommunication wavelength and uses a 10 ns pump pulse which corresponds to a spatial resolution of 1 m (Omnisens, 2019). This value could be reduced and thus increasing the sampling number of temperature spots along the FO cable, but the Brillouin gain (i.e. the magnitude of the backscattered light) would be reduced. The spatial resolution of 1 m is thus a reasonable compromise. Moreover, the sampling interval is 0.25 m and the temperature sensitivity is 0.2°C (Romanet et al., 2026).

FO-DTS data were collected between 2023-04-04 and 2023-04-11 in natural groundwater flow conditions. The fiber deployed at the experimental site is an industrial cable (external diameter of 4.8 mm) containing six optical fibers: four multi-mode fibers (MMF) and two single-mode fibers (SMF). the DITEST is connected to SMF fibers. This experiment is thus set up in a double-ended configuration, so we can measure Brillouin backscatter from both ends of the FO line (van de Giesen et al., 2012). The DITEST is therefore configured in Brillouin Optical Time Domain Analysis (BOTDA) mode because both ends of the FO cable need to be accessed. The raw measurement is an absolute frequency (GHz) and the DITEST performs a complete scan of the entire FO cable every two minutes. Optical losses were measured for the two SMF employed in this study and were 1.27 dB (slight defect at 222 m) and 0.055 dB, respectively, indicating reasonably low attenuation.

A Heatpulse (developed by *Silixa*) was connected to the FO cable (Fig. 3a and b) to increase the temperature signal of the fiber. In an Active-DTS experiment, the interpretation method is indeed based on the analysis of the thermal response curve. In that purpose, we locally removed about 15 cm of the plastic cladding protecting the fiber, allowing the electrical cable to be connected to the fiber's second protective cladding which is made of steel. This operation was carried out at three positions on the field setup (Fig. 3a). The electrical connection points between the HPS and the fiber are always located ahead of the heated fiber hole F3, F4 and F5, just before the fiber cable descends into the alluvial medium. These connections were protected in waterproof cases buried around 30 cm into the ground. Following several preliminary tests, the heating power rate has been set at 9 W/m (constant during the whole experiment) for F2, F3 and F4. F1 and F5 are not heated and are used as upstream and downstream controls (Fig. 1a) to ensure that the background groundwater temperature has remained stable during the acquisition period.

Two temperature-controlled baths have been placed at the beginning of the line (Fig. 3c), one is filled with ice and the other with water at ambient temperature. They are not strictly necessary for this experiment, they were not used as calibration baths but as local reference markers for locating positions along the FO cable which is 300 m long between the DITEST (placed at the beginning of the line) and the endpoint near F5 (Fig. 2). The groundwater level is also monitored in all piezometers with RuggedTroll 100 sensors (*In Situ Inc.*).

2.2.3.3. Data interpretation. The temperature of the fiber is determined with the temperature coefficient for a Single-Mode Fiber which is 1.07 MHz/K which allows the conversion of the absolute frequencies (GHz) into temperatures (°C). The experimental data interpretation is then based on the analysis of the thermal response curve which describes the increase of the FO temperature ΔT (°C) over time t (s) during the Active-DTS experiment. When the HPS is activated, the increase in temperature of the FO cable only depends on the thermal properties of the cable (at short times intervals). As a result, heat is accumulating in the FO cable and reaches eventually the surrounding saturated porous medium. In this phase, conduction controls the heat transfers between the FO cable and the porous medium. We expect to observe a plateau at later times (steady-state conditions where $\Delta T \approx 0$°C) meaning that advection now controls the dissipation of heat in the saturated medium (Selker and Selker, 2018; Simon et al., 2023; Simon and Bour, 2023).

The acquired dataset is then interpreted following the "A-DTS

Table 1
Summary of hydrological conditions during PDTs. The uncertainty given for the mean Doubs River discharge is the standard deviation during the time duration of the PDTs.

Tested well	Duration of the PDTs	Water height in the borehole (m)	Mean Doubs River discharge at Besançon (m^3/s)
PZ3	2022-04-21 to 04-22	3.9	40 ± 4
PZ5	2021-07-02 to 07-06	4.99	122 ± 2
PZ1	2021-07-02 to 07-06	5.36	122 ± 2
PZ7	2023-03-15 to 03-16	6.34	276 ± 33

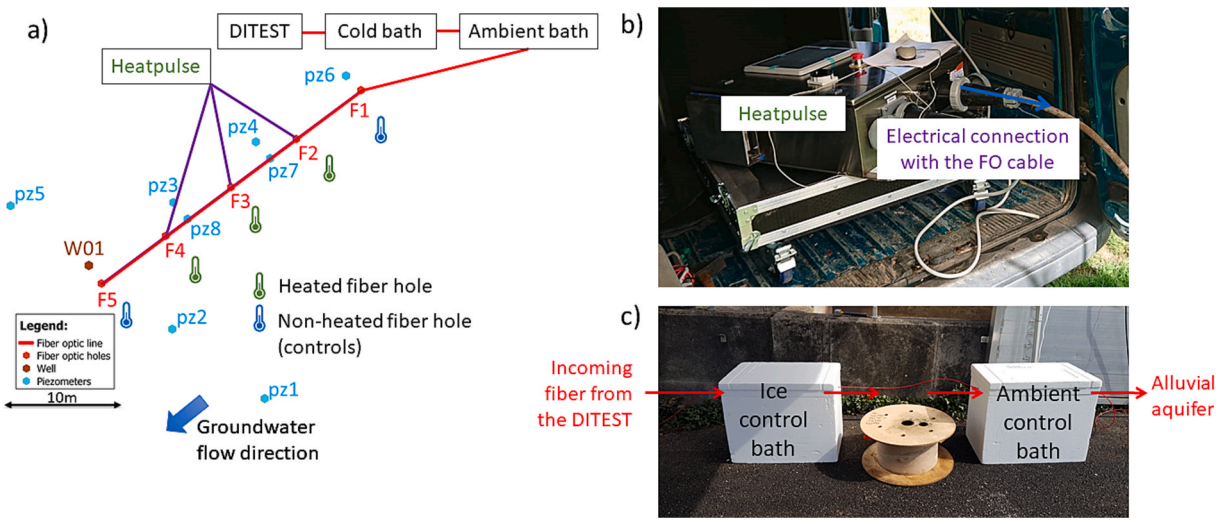

Fig. 3. (a) Field set-up deployed at the experimental site for the Brillouin active-DTS experiment in April 2023, (b) the Heatpulse System (HPS) used to increase the temperature signal in the FO cable at F2, F3, F4, the electrical connections are buried approximately 30 cm below the surface in waterproof boxes, allowing easier access if necessary, (c) pictures showing the two control baths for the FO temperature.

Toolbox" developed by Simon and Bour, (2023). This Toolbox includes a set of MATLAB codes which provides an automated interpretation of Active-DTS experiments, based on the Moving Instantaneous Line Source (MILS) model (4) (Carslaw and Jaeger, 1959). The toolbox allows the estimation of the thermal conductivities λ (W/m/K) of the material surrounding the FO cable and the groundwater fluxes q (m/s) for each measurement point located in the heated section of the fiber (F2, F3 and F4 in the present case), in the saturated porous media.

The MILS model is implemented in the toolbox to simulate the evolution of temperature ΔT_{PM} (°C) over time t (s) through the equation (4), ΔT_{PM} corresponds to the second and third phase of the thermal response curve.

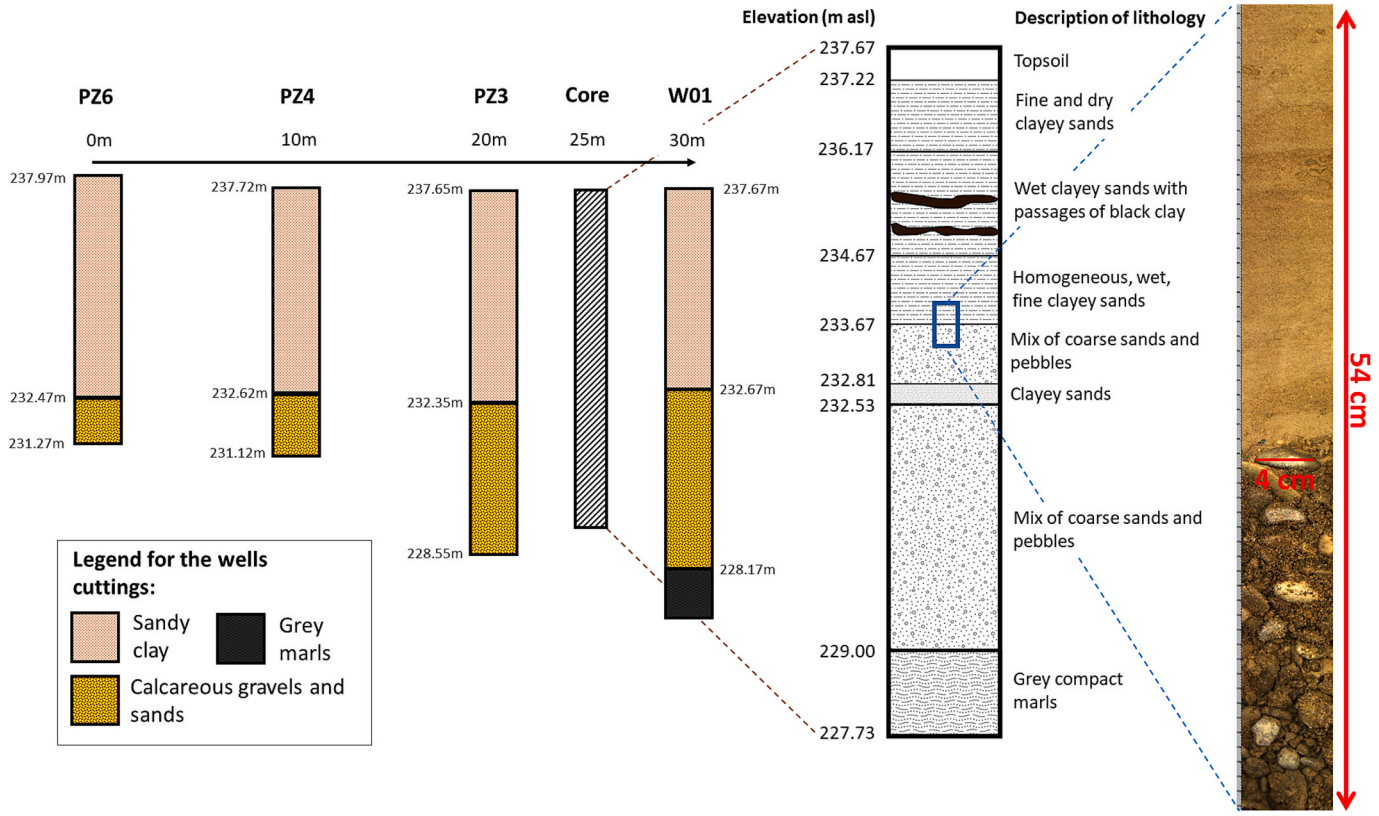

Fig. 4. Lithological description of the alluvial deposits at the experimental site of Port-Douvot given by the well cuttings (provided by the drilling company) and by the alluvial core sample. A high-resolution picture is given for a small portion of the core as an example to illustrate the transition between the different alluvium layers.

$$\Delta T_{PM}(x,y)=\frac{Q}{4\pi\lambda}exp\left[\frac{qx}{2D_t}\frac{\rho_w c_w}{\rho c}\right]\int_{\frac{x^2+y^2}{4tD_t}}^{\infty}exp\left[-\psi-\left(\frac{x^2+y^2}{D_t}\right)\frac{q^2}{16D_t\psi}\frac{\rho_{w^2}c_{w^2}}{\rho^2c^2}\right]\frac{d\psi}{\psi} \quad (4)$$

With q (m/s) the groundwater flux, Q (W/m) the heat power rate, ρc (J/m^3/K) the volumetric heat capacity of the rock-fluid matrix, $\rho_w c_w$ (J/m^3/K) the volumetric heat capacity of water, D_t (m^2/s) the thermal diffusivity coefficient that is also the ratio between the bulk thermal conductivity λ (W/m/K) and ρc, ψ is a change of variable. The coordinates x and y represent the distance from the heat source (located at x = 0 m and y = 0 m).

In step 1 of the Toolbox, the code 'Thermal conductivities estimates analytical MILS.m' is used to estimate the thermal conductivities λ (W/m/K) of the material around the FO cable, in which the flux q is fixed at 0 m/s. Then, the code 'Fluxes estimates analytical MILS.m' is used to estimate the groundwater fluxes q (m/s) along the heated section of the FO cable (step 2).

3. Results

3.1. Vertical and lateral heterogeneities in alluvial deposits

The vertical heterogeneities are identified by the alluvial core extracted from the experimental site between PZ3 and W01 (Fig. 4). Below 45 cm of topsoil, a layer of very fine clayey sands, sometimes wet, lies from 237.22 masl to 233.67 masl. Layers of darker, more compact clays are intercalated over 20–30 cm of thickness on the portion between 236.17 masl and 234.67 masl. Below 233.67 masl and down to 229.00 masl, a mixture of coarse alluvium is present with dominantly gravel-sand pebbles with an average diameter of 5–6 cm. Most of the sands and gravels encountered are clean, but some are embedded in a fine clay-textured matrix. A picture of a portion of the core is shown as an example (Fig. 4) highlighting the sharp transition between the homogeneous layer of clayey sands and the coarser alluvium. This abrupt change in grain size is located at 233.67 masl. The lateral heterogeneities are illustrated by Fig. 5, reporting the ERT cross-section that was obtained with a RMS of 1.4% after 5 iterations. The modeled resistivities range from 30 to 200 O-m. Low resistivities (30–100 O-m) are localized in the upper part of the subsoil between 238 and 235 masl (at PZ6) on the NE side and between 238 and 233.5 masl on the SW side of the panel (at PZ3). The low resistivities at the base of the panel correspond to the marl substratum, its depth increases by 3 m from NE to SW, or from 232 masl at 12 m to 229 masl at 42 m in terms of elevations. A layer of higher resistivity is continuously present along the entire profile (130–200 O-m), between 237 and 234 masl on the NE side and from 233 to 229 masl on the SW side.

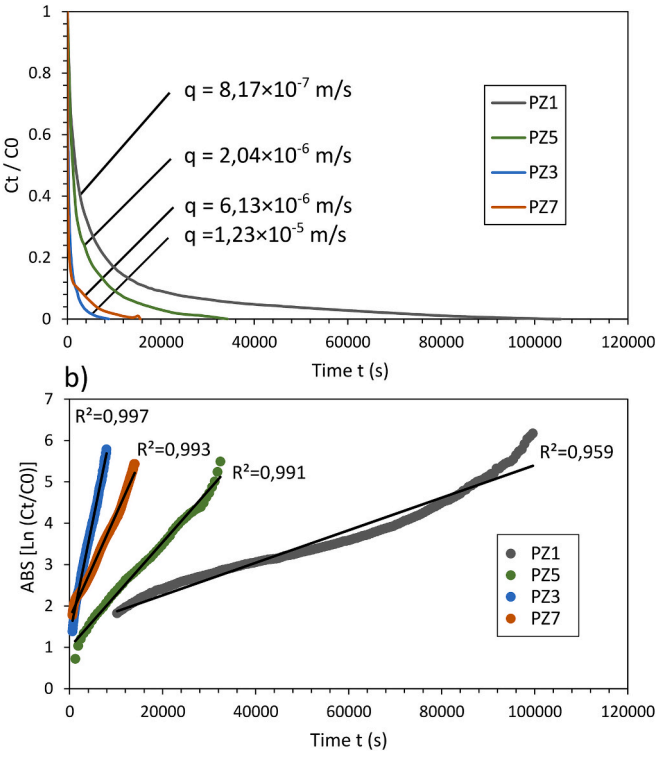

Fig. 6. (a) Restitution curves for the Point Dilution Tests (PDT) carried out for pz1, pz5, pz3, pz7 representing C_t/C_0 over time t (s), the interpreted fluxes q (m/s) are given, (b) absolute value of the natural logarithm (LN) of C_t/C_0 over time t (s) with the linear regression curves and their respective coefficient of determination R^2.

3.2. Groundwater fluxes by Point dilution tests

The restitution curves of the PDTs are presented in Fig. 6a where the

Table 2
Interpretation of the PDTs: initial concentration C_0 (g/l), the corrected EC (from $EC_{Background}$) at t = 0 s (µS/cm), apparent velocity V_a (m/s) and the Darcy velocity q (m/s).

Borehole	C0 (g/l)	Peak EC (µs/cm)	Va	q (m/s)
PZ3	67.8	68 350	2.45E−05	1.23E−05
PZ5	65.7	21 040	4.08E−06	2.04E−06
PZ1	61.9	52 237	1.63E−06	8.15E−07
PZ7	82.5	59 430	1.23E−05	6.15E−06

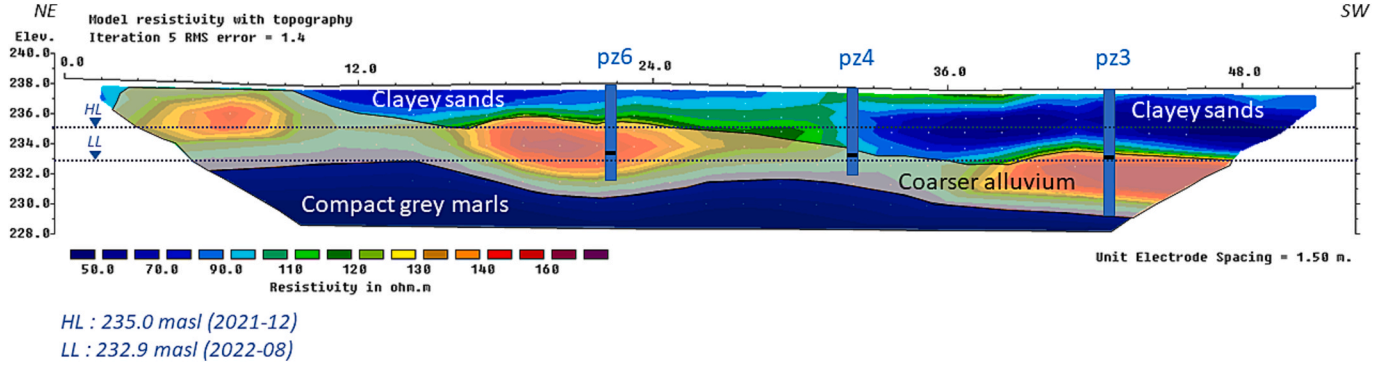

Fig. 5. Electrical resistivity panel parallel to the Doubs River whose location is shown in Fig. 1b, carried-out on the experimental site of Port-Douvot in October 2021, inverted with RES2DINV. Piezometers pz6, pz4 and pz3 are represented on the ERT panel. Average groundwater High-level (HL) and Low-Level (LL) are shown in the panel.

evolution of the saline tracer concentration C_t (g/l) over time t (s) has been normalized by the initial concentration C_0 (g/l). At time $t = 0$ s (Fig. 6a), $C_t = C_0$ and it matches the EC peak measured by the CTD-Divers (Table 2) which has been corrected by $EC_{background}$ which varies between 450 and 600 µS/cm. Fig. 6b shows the LN(C_t/C_0) curves (in absolute values) whose slope allows the estimation of V_a (Eq. (2)). The coefficients of determination R^2 all give satisfactory values above 0.99.

The rate at which EC (and thus C_t) returns to the level of $EC_{background}$ is proportional to the groundwater flux (Fig. 6a): the full recovery took 2.45 h for PZ3, 4.33 h for PZ7, 9.5 h for PZ5 and 28 h for PZ1. The calculated apparent velocities V_a (Table 2) cover a broad range from 1.63×10^{-6} m/s to 2.45×10^{-5} m/s as well as the values of the Darcy flux q that range from 8.17×10^{-7} m/s to 1.23×10^{-5} m/s (ratio of 15 between these two fluxes). PZ1, PZ5 and PZ7 are boreholes with similar depths and screened intervals from which we estimate an average groundwater flux q of 3.0×10^{-6} m/s (0.26 m/d). For this dataset, the calculated standard deviation is 2.27×10^{-6} m/s which is discussed later in this paper.

3.3. Groundwater fluxes by Brillouin active-DTS experiment

3.3.1. Temperature profile along the fiber optic cable

The evolution of the temperature in distance along the FO cable before heating and during heating is presented in Fig. 7a in accordance with the setup shown in Fig. 3a. The DITEST is located at distance 0 m and acquires data along the entire length of the FO cable. The "cold temperature bath" is located between 14 m and 22 m along the Distance axis of Fig. 7a and forms a plateau at 0°C which is expected. The "ambient temperature bath" forms a plateau as well, at 11.6°C between 26 m and 36 m. As illustrated by the Fig. 2, a large portion of the cable is not located in the saturated zone (but buried in the ground at the surface), these data are not analyzed in the case of this study (there are no groundwater fluxes in the unsaturated zone of the alluvial aquifer). Only the saturated sections located at F1, F2, F3, F4 and F5 (black arrows, Fig. 7a) are considered for data interpretation.

There is no significant difference in temperature on the controls (F1 and F5) between the pre-heating and the heating period (Fig. 7a) as expected. Likewise, F2, F3 and F4 respond correctly to heat injection (heating power of 9 W/m), thus the deployed setup on the field (Fig. 3a) is properly operating. The temperature peaks between 30°C and 50°C correspond to the electrical connections which overheat slightly but have no impact on the rest of the measurements in the saturated zone. In the case of F1 for instance (Fig. 7b), the temperature profile has a symmetrical shape because the FO cable makes a "U" shape loop at the bottom of F1 (Fig. 1d, Fig. 2), so the same temperature is measured on the downward and upward portions of the FO cable. This can also be applied to F2, F3, F4 and F5. Moreover, the total depth of F1 is 10.1 m, the FO section at 6°C (Fig. 7b) corresponds to the part of the cable located very close to the ground surface and approaching air temperature (mean air temperature on 2023–04-04 is 6.7°C). Then the FO temperature increases sharply to 10°C due to thermal inertia of the soil and stabilizes near the water-table. A change in slope is then observed as

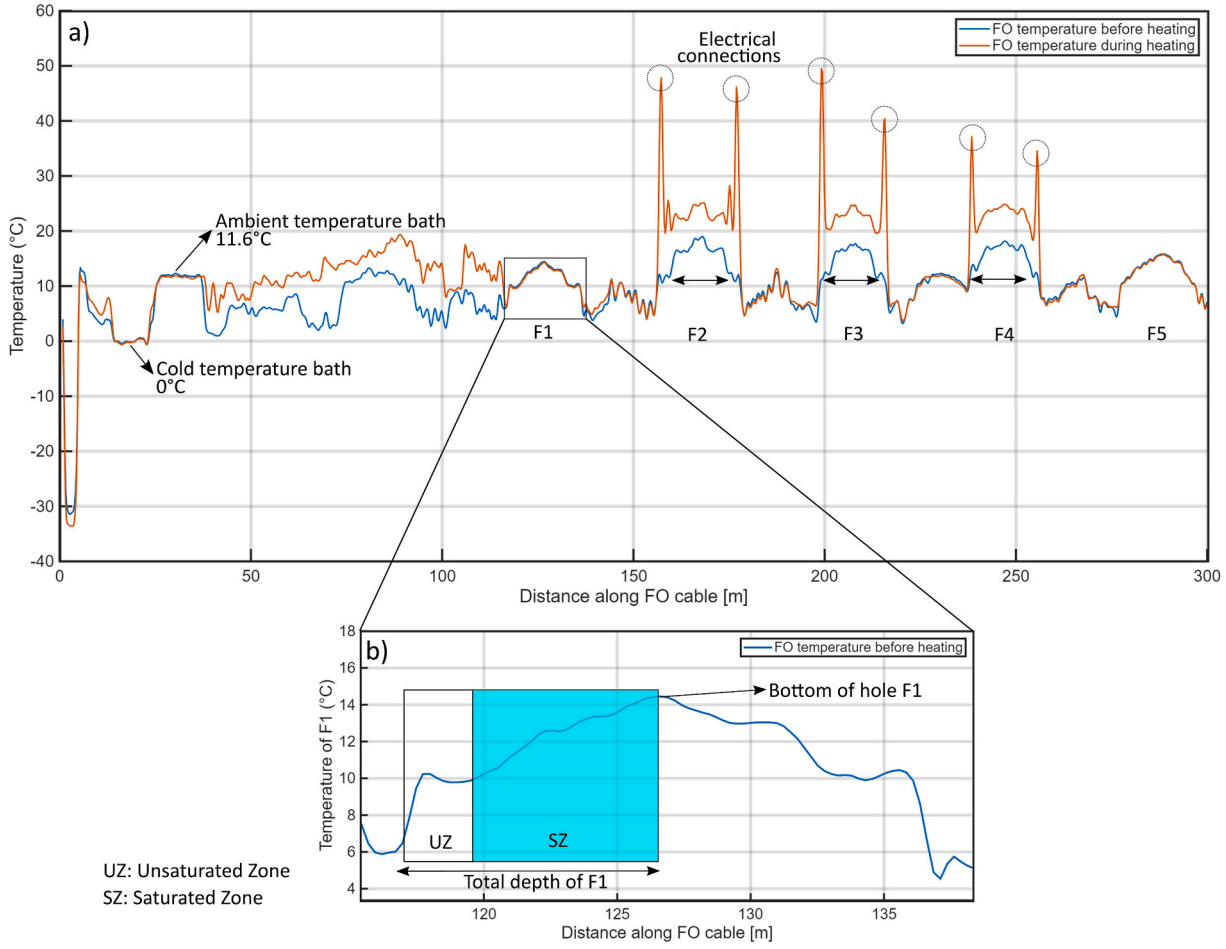

Fig. 7. a) Evolution of temperature (°C) along the FO cable as a function of distance [m] with the example of two cases: "before heating" (HPS not activated) and "during heating" (HPS activated at a heating power of 9 W/m). Specific sections of the FO cable are pointed out: the FO section passing through the "cold temperature bath", the section passing through the "ambient temperature bath" and which section corresponds to the FO holes (F1–F5) where the FO cable is vertically implanted in the alluvial aquifer, as shown in Fig. 2, b) zoom in the FO section corresponding to the control F1.

soon as the FO cable is located in the saturated zone of the alluvial aquifer, the FO temperature increasing with depth from 10°C to 14.4°C. This range of groundwater temperatures is confirmed by measurements from RBRsolo3 T located in piezometers at similar depths (on the same date of acquisition): the RBR in PZ6 located at 6 m depth indicates 12.47°C and that in PZ5 located at 9 m indicates 14.8°C. Indeed, it would be optimal to have a RBR sensor closer to the heated section of the FO cable to validate the temperature evolution in groundwater due to heating, but this is challenging to achieve in the field in an alluvial environment. The best configuration for now is to install temperature sensors in the piezometers nearest to the heated sections of the fiber. However, lab experiments carried out by Romanet et al. (2026) have shown that the current setup (BOTDA with SMF fibers) can perform measurements with a temperature uncertainty of ± 0.2°C.

3.4. Thermal response vs. time

The Fig. 8a illustrates the temperature variation (ΔT) of the FO cable as a function of time t at the bottom of F2, F3 and F4. Fig. 8b shows the evolution of temperature T as a function of time t for the controls F1 and F5. The temperature pattern is the same for each curve. When the HPS is activated, a sharp increase of 7-8°C is recorded during early times between 10^2 and 10^3 s (1 to ~15 mn) where temperature evolution is governed by the thermal properties of the FO cable (Simon and Bour, 2023). Between 10^3 s and 4×10^4 s (15 mn to ~11 h), the temperature rises more progressively, conduction controls heat transfers between the FO cable and the surrounding saturated porous medium. A steady-state is reached after ~28 h of heating where ΔT no longer increases meaning that advection is now controlling the evolution of FO temperature, the excess of heat is dissipated by groundwater fluxes. The entire heating phase has lasted 72 h. The mean FO temperature at the bottom of F1 and F5 has remained relatively stable during the heating phase (Fig. 8b) and was 13.91 ± 0.13°C for F1 and 15.27 ± 0.15°C for F5. At the same depth, the average temperature of F5 is indeed +1.36°C higher than F1, which can be explained by the distance separating F1 and F5 from the river. As F5 is further from the Doubs River (40 m) than F1 (28 m), the aquifer temperature is less influenced by colder surface waters (at this time of the year) and is thus slightly warmer (Molina-Giraldo et al., 2011).

3.5. Variations in depth of horizontal groundwater velocities

The variations of horizontal groundwater fluxes q (m/s) according to depth in the saturated zone (SZ) are presented in Fig. 9 for F2, F3 and F4. As seen in section 3.3.1., the temperature profile has a symmetrical shape for the downward and the upward section of the FO cable (Fig. 7), as a result, the flux profile is also symmetrical. Thus, for each flux measurement point located at the same elevation on the downward and upward section, we calculated an average and a standard deviation which are represented on Fig. 9. The thermal conductivities λ (W/m/K) were estimated using the MILS model along the heated section of the FO cable. For F2 to F4, the range of variation of thermal conductivities is 1 to 5 W/m/K (Fig. 9).

The fluctuations in groundwater fluxes appear consistent with the heterogeneities of alluvial deposits in depth. The average flux in the saturated zone is 3.8×10^{-7} m/s, 4.1×10^{-7} m/s and 3.3×10^{-7} m/s for F2, F3 and F4 respectively (Table 3). An increase in flux is observed between 232.5 masl and 229 masl which coincides with the presence of coarser materials as it was expected, but not of the same magnitude for F2, F3 and F4. For instance, the maximum estimated flux for F2 is 7.0×10^{-7} m/s (0.06 m/d) at 230.5 masl which corresponds to a relative variation of 84% with respect to the average flux (Table 3). Likewise, the maximum fluxes observed for F3 and F4 are 6.4×10^{-7} m/s and 7.0×10^{-7} m/s which correspond to a relative variation of 56% and 112%, respectively.

The F2 plot is the one with the largest standard deviations but is also the one that behaves most consistently with the lithology described by the core (Fig. 9). Between 234.5 and 233.5 masl, the aquifer material consists in homogeneous wet and fine clayey sands, the fluxes are at their lowest value of 2.1×10^{-7} m/s and then increase in the layer with

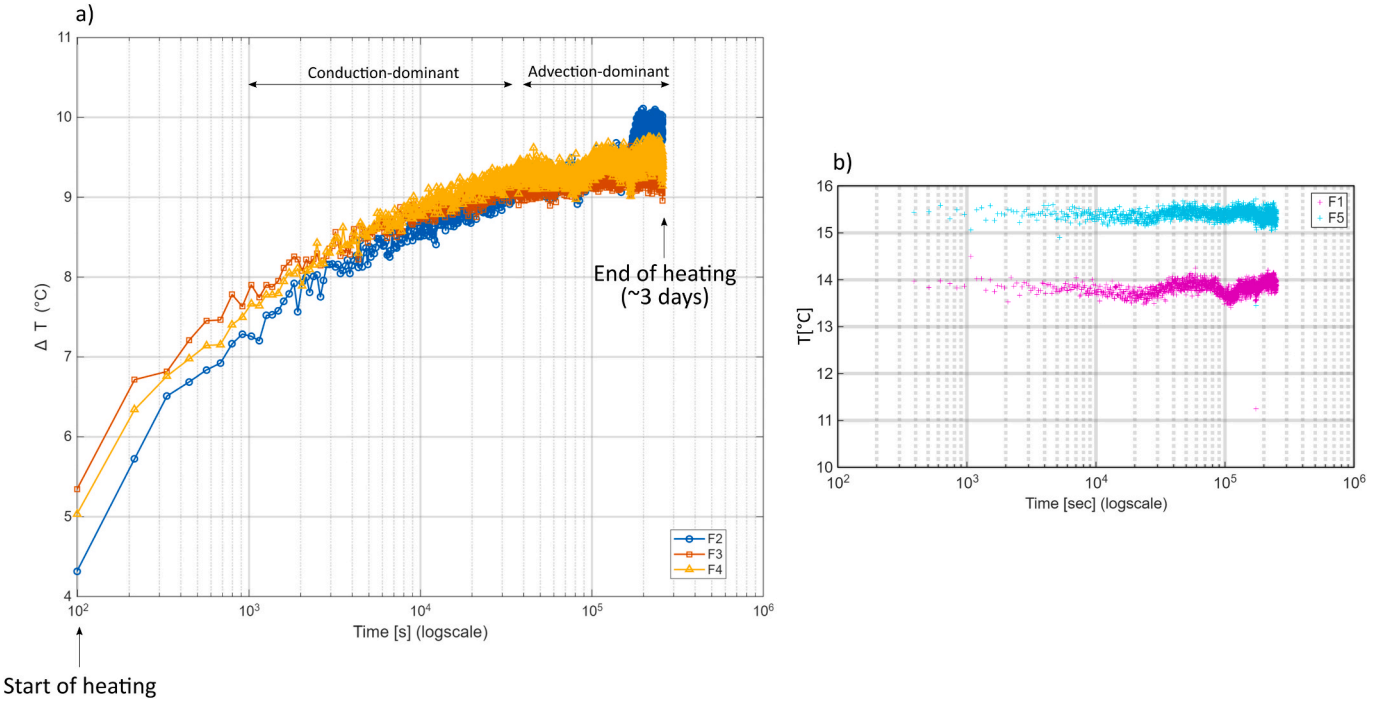

Fig. 8. a) Evolution of the temperature variation ΔT (°C) of the FO cable at the bottom of each heated FO hole (F2, F3 and F4) as a function of time (s), the curves are divided into 3 evolution steps: 1) heat is stored in the FO cable by conduction; 2) conduction controls heat transfer between the fiber and the surrounding saturated porous medium; 3) heat is dissipated by advection, b) evolution of the temperature T (°C) of the FO cable at the bottom of non-heated FO holes (F1 and F5) as a function of time (s), F1 and F5 are used as controls.

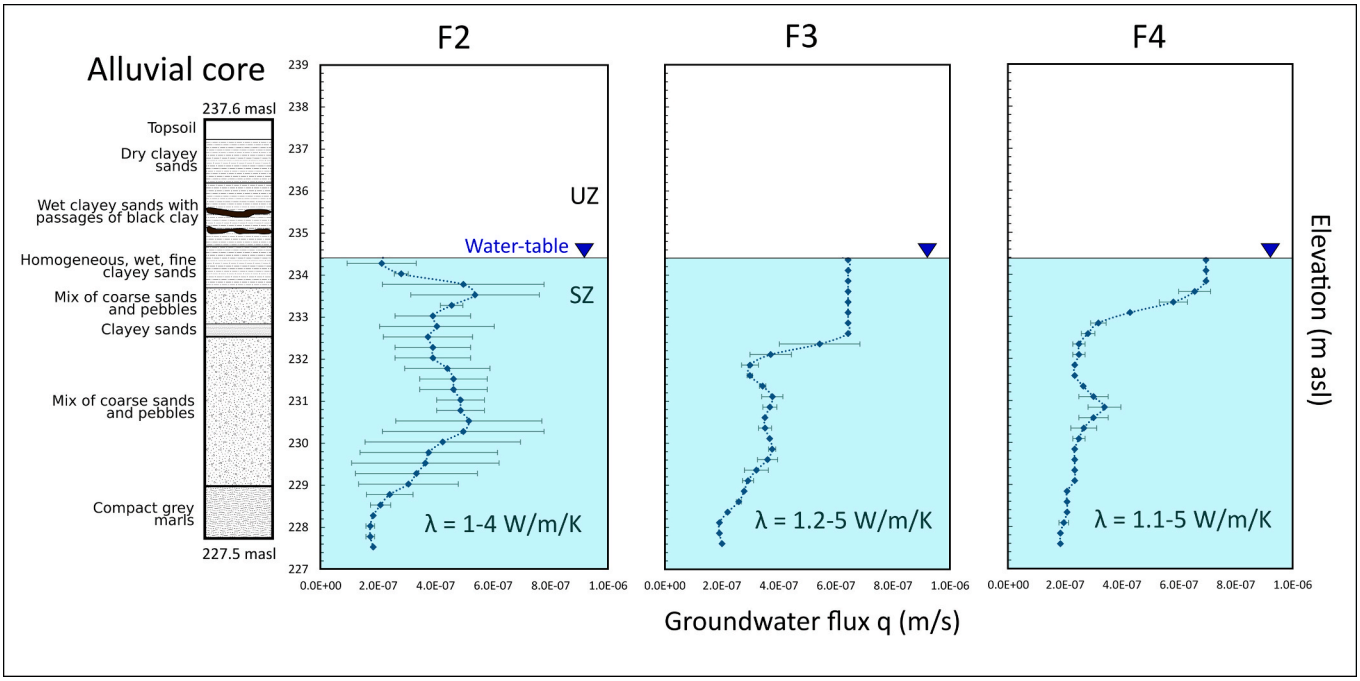

Fig. 9. Variation in depth (i.e. elevation in m asl) of horizontal groundwater fluxes q (m/s) interpreted for F2, F3 and F4 compared with the alluvial core (same vertical scale than the flux plots). Only values within the saturated zone were considered (values located in the vadose zone are not included in data interpretation). The set-up used gives us a flux value every 0.25 m. Horizontal bars represent the standard deviation. For each fiber hole Fx, it is the same fiber cable that ascends and descends (the cable forms a loop at the bottom of the borehole as illustrated by the Fig. 2), the same measurements were made on these two sections of cable. The interpreted fluxes are similar but not exactly the same, so the standard deviations shown in this figure are calculated using flux values at the same altitude on the two sections of the FO cable. The mean groundwater level (m asl) during the experiment is also illustrated and was 234.5 m asl (UZ: Unsaturated Zone, SZ: Saturated Zone).

Table 3
Summary of the groundwater fluxes estimated with the A-DTS method, the average, minimum (Min), maximum (Max) and the relative change (%) to the average of the Max flux value.

Flux q (m/s)	F2	F3	F4
Average	3.8E−07	4.1E−07	3.3E−07
MiN	1.7E−07	1.9E−07	1.8E−07
Max	7.0E−07	6.4E−07	7.0E−07
Relative change (%)	84.0	56.4	112.9

coarser grains. Around 232.6 m asl, the fluxes are decreasing again due to clay layers intercalated within the coarser alluviums. A portion of the marl substratum was drilled unintentionally over approximately 1.20 m, thus the bottom part of the fiber which is ballasted (Fig. 1d) lies in the bedrock. It occurs in conjunction with the decrease in fluxes between 230 and 227.5 m asl.

4. Discussion

4.1. Heterogeneities in space

The ERT survey has provided resistivity contrasts (Fig. 5) that match with the different alluvial layers observed on the core sample (Fig. 4). The upper part of the subsurface, the first 5 m at PZ3, consists of clayey sands with low resistivities (30–100 O-m) and the lower part is composed of coarser materials (gravels and pebbles in a matrix of sands) with higher resistivities (130–200 O-m). The range of observed resistivities in alluvial environments can be wide and vary considerably from one alluvial aquifer to another, but our values are compatible with the type of material encountered (Loke, 2004; Göktürkler et al., 2008; Gómez et al., 2019; Mishra et al., 2023). The data cross-checking between the core and the borehole logs (Fig. 4) and the ERT profile are consistent for PZ3, which is less the case for PZ6. Indeed, in the logs, the transition between fine and coarse alluvium is located at 232.5 masl, whereas in the ERT profile this transition is located at 235 masl, a difference of 2.5 m. Although the RMS is low (1.4%), this inconsistency is more likely to be due to an inversion artefact or an insufficient number of sampling points (“quadripoles” in RES2DINV), resulting in a lower resolution in the distribution in space of resistivities. It should be noted that these resistivity values are the result of an iterative modelling on RES2DINV and cannot reach the precision of a direct observation such as a core sampling.

The ERT cross-section and the core highlighted that vertical heterogeneity is more significant than lateral heterogeneity. Indeed, a fluvial system deposits successive horizontal layers of alluvium over time, forming a final tabular environment which is the case on the study site. Although these two techniques map different areas of the alluvial deposits, they produce consistent results. The alluvial core showed a distinct transition between the fine and the coarse deposits at 233.67 masl (Fig. 4) which matches correctly with the higher and the lower resistivity layers observed at the SW end of the ERT cross-section (Fig. 5). The core also shows heterogeneities at a sub-metric scale that are not visible on the ERT cross-section because this method is poorly suited to capture sub-metric variations in grain size, hence the interest in comparing these two methods. This sudden transition in grain size should have a strong influence on horizontal groundwater fluxes, the coarser deposits are supposedly responsible for the high hydraulic conductivity value of 5.10^{-2} m/s and may act as a preferential pathway for groundwater flow (Mulligan et al., 2007; McArthur et al., 2008; Samadder et al., 2011; Vogelgesang et al., 2020). We assume that this resistive layer at the base of the ERT profile might be a paleochannel that extends across the entire site. Moreover, the groundwater level of this alluvial aquifer is located in the coarser materials most of the time (below ‘HL’ on Fig. 5), especially during low-flows (Fig. 10). The value $K = 5.10^{-2}$ m/s was obtained from a pumping test carried out in April

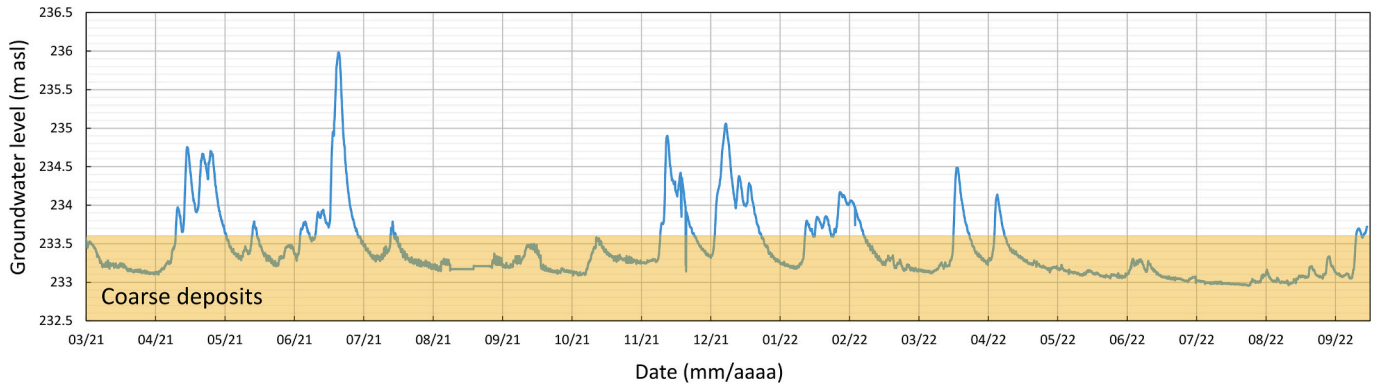

Fig. 10. Example of groundwater levels variation (m asl) in time of the alluvial aquifer at Port-Douvot from the CTD-Diver sensor in PZ6. The levels in the yellow part represent the moments when the groundwater level is located only in the coarse alluvial layer, during low-water periods mostly. (For interpretation of the references to colour in this figure legend, the reader is referred to the web version of this article.)

2023 when the groundwater level was located below the transition zone, thus reflecting the hydraulic properties of the coarser alluvium (W01 is screened in the coarse alluvial layer).

4.2. Variability of groundwater fluxes

When using an 'advanced' method such as A-DTS to estimate fluxes, it may be worthwhile to implement a less sophisticated method that produces results more quickly to discuss the reliability of the fluxes obtained with the 'advanced' method. The PDT technique was carried out with that purpose, as it is simple to conduct in the field and straightforward to interpret. The estimated PDT fluxes spanned a wide interval between 1.2×10^{-5} to 8.2×10^{-7} m/s (Fig. 11) with an average of 3.0×10^{-6} m/s (for PZ1, PZ5 and PZ7 that have the same screen intervals) while A-DTS fluxes fall within a shorter range, between 1.7×10^{-7} m/s (F2) and 7.0×10^{-7} m/s (F2, F4). Indeed, the maximum value obtained by PDT is 15 times higher than the observed minimum (Table 3) whereas this same ratio is only between 3 and 4 for A-DTS fluxes. We can first analyze the plausibility of such fluxes in an alluvial environment and then their consistency relative to the method. To begin with, estimated groundwater fluxes in alluvial aquifers are highly variable from one site to another, but the values we have interpreted by PDT and A-DTS are consistent with those reported in the literature (Fig. 11): 2.14×10^{-7} to 9.84×10^{-6} m/s (Piccinini et al., 2016), 4.05×10^{-6} to 6.02×10^{-4} m/s (Jamin and Brouyère, 2018), 8.10×10^{-7} to 1.24×10^{-5} m/s (Perzan and Chapin, 2023). These wide ranges of fluxes highlight the structural heterogeneity of alluvial aquifers and their complex flow-field (Dogan et al., 2014; Dey et al., 2021; Yin et al., 2023).

However, given the "simplicity" of the PDT technique, it is challenging to clearly relate the variations in groundwater flux from one borehole to another with spatial heterogeneity of alluvial deposits, especially since this method only provides a single value. Various factors

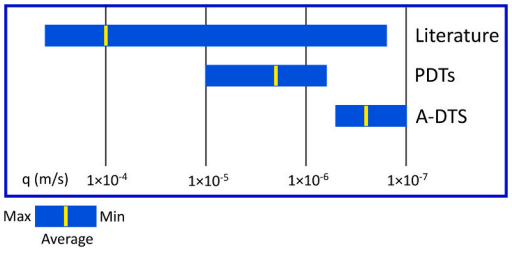

Fig. 11. Comparison of the groundwater fluxes values from literature in alluvial aquifers (Piccinini et al., 2016; Jamin and Brouyère, 2018; Perzan and Chapin, 2023), from the PDTs (Fig. 6) and the A-DTS carried out on the experimental site of Port-Douvot (Fig. 9).

can influence the quality of the PDT results: the choice of the injection method (Fahrmeier et al., 2021), the water recirculation system (Lamontagne et al., 2002) or density effects by using a saline solution (Shafer et al., 2010). Moreover, the LN(C_t/C_0) curves used to interpret the PDTs are acceptable (Fig. 6b), but the PZ1 curve for instance, shows some disturbances that may be due to the proximity of the Doubs River or to the mixing of the tracer throughout the test which might also explain the dispersion of the flux values around the average (as seen in section 3.2).

The use of A-DTS allows to overcome the limitations of conventional methods such as PDT. The estimated fluxes q are obtained after the calculation of the thermal conductivities computed by the MILS model that yielded values between 1 and 5 W/m/K. Although this interval of λ is relatively wide, it remains consistent with values reported in the literature for a medium consisting of saturated sand, gravel and pebbles (Stauffer et al., 2013; Wildemeersch et al., 2014; Albers et al., 2024). One important point is that the variation of groundwater fluxes q in depth is consistent with vertical heterogeneities (Fig. 9) identified in the alluvial deposits (Figs. 4 and 5). Although the A-DTS flux values are at the lower bound of the typical observed range (Fig. 11), they remain within plausible limits. However, the proximity of these fluxes to the detection limits of the A-DTS warrants caution. Indeed, experiments conducted by Simon et al., (2021) in a homogeneous sandbox showed that the A-DTS approach may provide fluxes from 1×10^{-6} to 5×10^{-2} m/s (after 4 h of heating). It can be reasonably assumed that flux ranges estimated under field conditions in a heterogeneous anisotropic medium may slightly differ from those obtained under controlled experimental conditions. For a heat duration t (constant over time) and if the background temperature has remained stable, the time required to reach a thermal steady-state depends on the magnitude of groundwater fluxes (Diao et al., 2004; Simon et al., 2023). During the Brillouin A-DTS experiment, no significant change in background temperature was recorded and hydrological conditions remained stable (no variation in groundwater levels, no precipitation that could have introduced a vertical flow component). However, a key factor that may affect the evolution of ΔT in the FO cable and therefore the estimated λ (W/m/K) and q (m/s) values, is the backfilling of the fiber holes after their installation (F1 to F5). This process controls the "quality" of the contact between the FO cable and the surrounding alluvial medium. Bakker et al., (2015) have installed FO cables vertically, as we did, but using a direct push technique instead of drilling a hole. This approach allows a direct contact between the FO cable and the aquifer material, and reduces flow disturbances. While this technique could be considered in our case (for a future experiment), field observations during drilling of F1 to F5 revealed that the alluvial medium is not as unconsolidated as anticipated. The manner in which the fiber is installed within the aquifer material is therefore a critical aspect of A-DTS experiments.

The observed variations in flux q as a function of depth observed in this study are smooth and progressive (Fig. 9). The behavior we are examining here in a saturated porous medium is different from what we might observe in a fractured aquifer for instance, with more abrupt flow changes with depth (Read et al., 2013; Munn et al., 2020; Maldaner et al., 2021). In our study case, the entire thickness of the saturated zone contributes to the flow at different velocities depending on the hydraulic properties of the alluvial deposits. Moreover, it should be noted that this A-DTS test was carried out under natural groundwater flow conditions. Setting up pumping conditions may have advantages, the advective phase should be reached in less time and higher fluxes could be measured.

4.3. Added value of using Brillouin backscattering

A Brillouin-based sensor was successfully used in this study to estimate groundwater fluxes in an alluvial aquifer. Nevertheless, as with all sensors of this type, it exhibits both strengths and limitations which are discussed hereafter. One of the major benefits of this method is that the Brillouin scatter is a frequency-based measurement (Romanet, 2024), the Brillouin Frequency Shift (BFS) being linearly correlated to temperature (Nikles et al., 1997). Within a single FO cable, optical losses (expressed in dB) of varying magnitude may occur due to the different splices and connections made by the user. These losses affect the intensity of the backscattered signal but not the BFS (Bao et al., 2021), unlike Raman for which the attenuation of signal intensity has drawbacks on the accuracy of temperature measurements (Li and Zhang, 2022). In the case of Raman, a calibration is required in the field (using temperature-controlled baths) to ensure the precision of temperature measurements over time (Hausner et al., 2016), which is not the case for Brillouin-based sensors. Indeed, knowing the BFS as a function of temperature and a frequency reference measured in laboratory at a known temperature, we were therefore able to interpret temperatures along the FO cable from absolute frequency measurements without any field-calibration (Hartog, 2017). However, since the DITEST performs a frequency scan and measures both temperature and strain, the acquisition time is longer, between 3 and 5 min or 5 to 15 min for high resolution measurements (Omnisens, 2019). Indeed, Brillouin backscatter is sensitive to both fiber temperature and strain. Measured temperatures are affected in consequence if the FO cable is subjected to strain. In this study, we therefore used a tube loose-fiber (Bastianini et al., 2019) in which one fiber is loose and dedicated to temperature sensing only while other is attached to the structure and is sensitive to temperature and strain. Furthermore, different studies have already demonstrated the ability of accurate Brillouin measurements to be carried out over long distances ranging from 50 to 150 km (Bao and Chen, 2011; Fu et al., 2018; Kapa et al., 2018). This feature offers new possibilities for the monitoring of environmental parameters such as river/groundwater interactions over long distances for instance, or the monitoring of strain in various infrastructures (buildings, roads, brides etc.).

Despite their robustness, A-DTS methods require extensive field logistics (fiber installation, observation boreholes, water loggers and temperature sensors, heatpulse, DTS unit, computers) etc. and thus rely on a stable source of electricity. That is why the ability of this DTS technology to provide absolute measurements over long distances is of significant interest in hydrogeology, particularly for long-term passive monitoring applications. Moreover, one of the major remaining challenges is the spatial resolution. A resolution of 1 m may be a considerable limitation when the thickness of the saturated zone is only a few meters as it restricts the number of interpretable sampling points. In our case study, the saturated zone is 5 to 6 m thick which turned out to be just enough for this experiment. Further advances need to be made to improve this parameter and reduce it down to the centimeter scale, which would be optimal in the case of alluvial aquifers. For instance, a centimeter-scale resolution would provide valuable insights into the effects of granular heterogeneity on groundwater fluxes. This has already been achieved, but only in laboratory experiments (Bersan et al., 2017; Gasser et al., 2022). This topic will be the subject of future investigations.

5. Conclusion

In this study, we explored the use of a Brillouin-based sensor (DITEST) to perform active distributed temperature measurements with the objective of estimating groundwater fluxes under natural groundwater flow conditions. The method is based on the linear relationship between the Brillouin Frequency Shift (GHz) and fiber temperature (°C). The DITEST measures absolute frequency data along a fiber optic cable with a spatial resolution of 1 m, a sampling interval of 0.25 m and a temperature sensitivity of 0.2°C. No temperature-controlled baths are required to carry out Brillouin backscatter measurements, control baths were used only as reference points along the fiber. Temperatures measured along the fiber optic cable through the use of Brillouin backscatter were consistent with groundwater temperatures recorded by RBRsolo3 T sensors. These findings indicate that our field setup performs as expected and can be used again for future experiments. An Electrical Resistivity Tomography cross-section was carried out and a 10 m depth core sample was extracted to investigate the lateral and vertical heterogeneities of the alluvial deposits. We showed that the vertical distribution of horizontal groundwater fluxes were consistent with subsurface heterogeneities. Point Dilution Tests (PDT) using common salt (NaCl) were conducted to assess the range of possible groundwater fluxes in our study area, A-DTS–derived fluxes fall within the lower range estimated by PDTs but remain plausible. To the best of our knowledge, it was the first time that a Brillouin-based sensor was deployed in the field to estimate groundwater fluxes in an alluvial aquifer. Additional work is required to better define the limitations of this method. Lastly, investigations comparing the precision and resolution of Brillouin vs. Raman are currently underway.

CRediT authorship contribution statement

Jordan Labbe: Writing – original draft, Methodology, Formal analysis. **Maxime Romanet:** Software, Methodology, Formal analysis, Data curation. **Hélène Celle:** Writing – review & editing, Supervision, Methodology, Funding acquisition, Conceptualization. **Maxime Zerbib:** Investigation. **Kien Phan Huy:** Writing – original draft, Methodology, Conceptualization. **Alexandre Matic:** Software, Methodology, Investigation, Formal analysis, Data curation. **Victor Klaba:** Investigation. **Gilles Mailhot:** . **Jean-Charles Beugnot:** Writing – review & editing, Supervision, Methodology, Funding acquisition, Conceptualization.

Funding

This work was funded by both SENSAAS (SENSors and Analyses for AquiferS, funding source: PIA3 UBFC) and GOOFI (Groundwater Observations through Optic Fiber Investigations, funding source: Région Bourgogne Franche-Comté) projects.

Declaration of competing interest

The authors declare that they have no known competing financial interests or personal relationships that could have appeared to influence the work reported in this paper.

Acknowledgments

We express our sincere gratitude to Olivier Bour and Nathaline Simon (University of Rennes) for their help and their many advices which allowed us to improve our experiments. We would also like to thank all the staff at the Port-Douvot wastewater treatment plant (Grand Besançon Metropole) for allowing us to use their infrastructure and

electricity, and in particular John Guerittot for his invaluable technical assistance.

Data availability

The collected data in this study are available at the following DOI link on the H + database: https://doi.org/10.26169/hplus.portdouvot_brillouin_a-dts_experiment_2023

References

Albers, A., Steger, H., Zorn, R., Blum, P., 2024. Evaluating an enhanced thermal response test (ETRT) with high groundwater flow. Geotherm. Energy 12. https://doi.org/10.1186/s40517-023-00278-y.

Anderson, M.P., 2005. Heat as a Ground Water Tracer. Groundwater 43, 951–968. https://doi.org/10.1111/j.1745-6584.2005.00052.x.

Bakker, M., Caljé, R., Schaars, F., Van Der Made, K., De Haas, S., 2015. An active heat tracer experiment to determine groundwater velocities using fiber optic cables installed with direct push equipment. Water Resour. Res. 51, 2760–2772. https://doi.org/10.1002/2014WR016632.

Banks, E.W., Morgan, L.K., Sai Louie, A.J., Dempsey, D., Wilson, S.R., 2022. Active distributed temperature sensing to assess surface water–groundwater interaction and river loss in braided river systems. J. Hydrol. 615, 128667. https://doi.org/10.1016/j.jhydrol.2022.128667.

Bao, X., Chen, L., 2011. Recent progress in optical fiber sensors based on Brillouin scattering at university of Ottawa. Photonic Sens 1, 102–117. https://doi.org/10.1007/s13320-011-0026-3.

Bao, X., Webb, D.J., Jackson, D.A., 1993. 22-km distributed temperature sensor using Brillouin gain in an optical fiber. Opt. Lett. 18, 552. https://doi.org/10.1364/OL.18.000552.

Bao, X., Zhou, Z., Wang, Y., 2021. Review: distributed time-domain sensors based on Brillouin scattering and FWM enhanced SBS for temperature, strain and acoustic wave detection. PhotoniX 2, 14. https://doi.org/10.1186/s43074-021-00038-w.

Bastianini, F., Di Sante, R., Falcetelli, F., Marini, D., Bolognini, G., 2019. Optical fiber sensing cables for brillouin-based distributed measurements. Sensors 19, 5172. https://doi.org/10.3390/s19235172.

Bersan, S., Schenato, L., Rajendran, A., Palmieri, L., Cola, S., Pasuto, A., Simonini, P., 2017. Application of a high resolution distributed temperature sensor in a physical model reproducing subsurface water flow. Measurement 98, 321–324. https://doi.org/10.1016/j.measurement.2015.09.018.

Boyd, C.D., Dickerson, B.D., Fitzpatrick, B.K., 2011. Monitoring distributed temperatures along superconducting degaussing cables via Rayleigh backscattering in optical fibers.

Butler, J.J., 1990. The role of pumping tests in site characterization: some theoretical considerations. Groundwater 28, 394–402. https://doi.org/10.1111/j.1745-6584.1990.tb02269.x.

Carslaw, H.S., Jaeger, J.C., 1959. Conduction of heat in solids., Oxford University. Oxford (UK).

Chai, Q., Luo, Y., 2019. Review on fiber-optic sensing in health monitoring of power grids. Opt. Eng. 58, 1. https://doi.org/10.1117/1.OE.58.7.072007.

Coleman, T.I., Parker, B.L., Maldaner, C.H., Mondanos, M.J., 2015. Groundwater flow characterization in a fractured bedrock aquifer using active DTS tests in sealed boreholes. J. Hydrol. 528, 449–462. https://doi.org/10.1016/j.jhydrol.2015.06.061.

Dann, R.L., Close, M.E., Pang, L., Flintoft, M.J., Hector, R.P., 2008. Complementary use of tracer and pumping tests to characterize a heterogeneous channelized aquifer system in New Zealand. Hydrgeol. J. 16, 1177–1191. https://doi.org/10.1007/s10040-008-0291-4.

Dashti, Z., Nakhaei, M., Vadiati, M., Karami, G.H., Kisi, O., 2022. A literature review on pumping test analysis (2000–2022). Environ. Sci. Pollut. Res. 30, 9184–9206. https://doi.org/10.1007/s11356-022-24440-4.

Derouane, J., Dassargues, A., 1998. Delineation of groundwater protection zones based on tracer tests and transport modeling in alluvial sediments. Environ. Geol. 36, 27–36.

Dey, S., Shukla, U.K., Mehrishi, P., Mall, R.K., 2021. Appraisal of groundwater potentiality of multilayer alluvial aquifers of the Varuna river basin, India, using two concurrent methods of MCDM. Environ. Dev. Sustain. 23, 17558–17589. https://doi.org/10.1007/s10668-021-01400-5.

Diao, N., Li, Q., Fang, Z., 2004. Heat transfer in ground heat exchangers with groundwater advection. Int. J. Therm. Sci. 43, 1203–1211. https://doi.org/10.1016/j.ijthermalsci.2004.04.009.

Dogan, M., Van Dam, R.L., Liu, G., Meerschaert, M.M., Butler, J.J., Bohling, G.C., Benson, D.A., Hyndman, D.W., 2014. Predicting flow and transport in highly heterogeneous alluvial aquifers. Geophys. Res. Lett. 41, 7560–7565. https://doi.org/10.1002/2014GL061800.

Domenico, P.A., Schwartz, F.W., 1998. Physical and chemical hydrogeology, 2. ed., paperback. ed. Wiley, New York Chichester Weinheim.

Drost, W., Klotz, D., Koch, A., Moser, H., Neumaier, F., Rauert, W., 1968. Point dilution methods of investigating ground water flow by means of radioisotopes. Water Resour. Res. 4, 125–146. https://doi.org/10.1029/WR004i001p00125.

Fahrmeier, N., Goeppert, N., Goldscheider, N., 2021. Comparative application and optimization of different single-borehole dilution test techniques. Hydrgeol. J. 29, 199–211. https://doi.org/10.1007/s10040-020-02271-2.

Freeze, R.A., Cherry, J.A., 1979. Groundwater. Prentice-Hall, Englewood Cliffs, N.J.

Fu, Y., Wang, Z., Zhu, R., Xue, N., Jiang, J., Lu, C., Zhang, B., Yang, L., Atubga, D., Rao, Y., 2018. Ultra-long-distance hybrid BOTDA/Φ-OTDR. sensors 18, 976. https://doi.org/10.3390/s18040976.

Furlanetto, D., Camporese, M., Schenato, L., Costa, L., Salandin, P., 2024. Fiber optics passive monitoring of groundwater temperature reveals three-dimensional structures in heterogeneous aquifers. Sci. Rep. 14. https://doi.org/10.1038/s41598-024-58954-3.

Galindez-Jamioy, C.A., López-Higuera, J.M., 2012. Brillouin distributed fiber sensors: an overview and applications. J. Sensors 2012, 1–17. https://doi.org/10.1155/2012/204121.

Gasser, J., Warpelin, D., Bussières, F., Extermann, J., Pomarico, E., 2022. Distributed temperature sensor combining centimeter resolution with hundreds of meters sensing range. Opt. Express 30, 6768. https://doi.org/10.1364/OE.451699.

Göktürkler, G., Balkaya, Ç., Erhan, Z., Yurdakul, A., 2008. Investigation of a shallow alluvial aquifer using geoelectrical methods: a case from Turkey. Environ. Geol. 54, 1283–1290. https://doi.org/10.1007/s00254-007-0911-7.

Gómez, E., Larsson, M., Dahlin, T., Barmen, G., Rosberg, J.-E., 2019. Alluvial aquifer thickness and bedrock structure delineation by electromagnetic methods in the highlands of Bolivia. Environ. Earth Sci. 78, 84. https://doi.org/10.1007/s12665-019-8074-x.

Guzowski, B., Lakomski, M., Bobinski, D., 2025. Hotspot detection in photovoltaic modules with fiber Bragg grating and Brillouin distributed temperature sensors. Energies 18, 6117. https://doi.org/10.3390/en18236117.

Hartog, A.H., 2017. An Introduction to Distributed Optical Fibre Sensors, 1st ed. Taylor & Francis Group CRC Press, Boca Raton.

Hausner, M.B., Kryder, L., Klenke, J., Reinke, R., Tyler, S.W., 2016. Interpreting variations in groundwater flows from repeated distributed thermal perturbation tests. Groundwater 54, 559–568. https://doi.org/10.1111/gwat.12393.

Hermans, T., Goderniaux, P., Jougnot, D., Fleckenstein, J.H., Brunner, P., Nguyen, F., Linde, N., Huisman, J.A., Bour, O., Lopez Alvis, J., Hoffmann, R., Palacios, A., Cooke, A.-K., Pardo-Álvarez, Á., Blazevic, L., Pouladi, B., Haruzi, P., Fernandez Visentini, A., Nogueira, G.E.H., Tirado-Conde, J., Looms, M.C., Kenshilikova, M., Davy, P., Le Borgne, T., 2023. Advancing measurements and representations of subsurface heterogeneity and dynamic processes: towards 4D hydrogeology. Hydrol. Earth Syst. Sci. 27, 255–287. https://doi.org/10.5194/hess-27-255-2023.

Jamin, P., Brouyère, S., 2018. Monitoring transient groundwater fluxes using the Finite Volume Point Dilution Method. J. Contam. Hydrol. 218, 10–18. https://doi.org/10.1016/j.jconhyd.2018.07.005.

Joshua, T.J., Daniel, C.S., Anthony, B., Christian, M.P., Thomas, E.B., 2022. Calibration of distributed temperature sensors using commercially available SMF-28 optical fiber from 22 °C to 1000 °C. IEEE Sens. J. 22, 4144–4151.

Kapa, T., Schreier, A., Krebber, K., 2018. 63 km BOFDA for temperature and strain monitoring. Sensors 18, 1600. https://doi.org/10.3390/s18051600.

Klepikova, M., Wildemeersch, S., Hermans, T., Jamin, P., Orban, P., Nguyen, F., Brouyère, S., Dassargues, A., 2016. Heat tracer test in an alluvial aquifer: Field experiment and inverse modelling. J. Hydrol. 540, 812–823. https://doi.org/10.1016/j.jhydrol.2016.06.066.

Kollet, S.J., Zlotnik, V.A., 2003. Stream depletion predictions using pumping test data from a heterogeneous stream–aquifer system (a case study from the Great Plains, USA). J. Hydrol. 281, 96–114. https://doi.org/10.1016/S0022-1694(03)00203-8.

Lamontagne, S., Dighton, J., Ullman, W., 2002. Estimation of groundwater velocity in riparian zones using point dilution tests (No. Technical Report 14/02). CSIRO Land and Water.

Li, J., Zhang, M., 2022. Physics and applications of Raman distributed optical fiber sensing. Light Sci. Appl. 11, 128. https://doi.org/10.1038/s41377-022-00811-x.

Loke, M.H., 2004. Tutorial : 2-D and 3-D electrical imaging surveys.

Loke, M.H., Barker, R.D., 1996. Rapid least-squares inversion of apparent resistivity pseudosections by a quasi-newton method. Geophys. Prospect., Eur. Assoc. Geosci. Eng. 44, 131–152.

Maldaner, C.H., Munn, J.D., Green, B.A., Warner, S.L., Chapman, S.W., Ashton, A., Daubert, L., Parker, B.L., 2021. Quantifying groundwater flow variability in a poorly cemented fractured sandstone aquifer to inform in situ remediation. J. Contam. Hydrol. 241, 103838. https://doi.org/10.1016/j.jconhyd.2021.103838.

McArthur, J.M., Ravenscroft, P., Banerjee, D.M., Milsom, J., Hudson-Edwards, K.A., Sengupta, S., Bristow, C., Sarkar, A., Tonkin, S., Purohit, R., 2008. How paleosols influence groundwater flow and arsenic pollution: a model from the Bengal Basin and its worldwide implication: arsenic in groundwater. Water Resour. Res. 44. https://doi.org/10.1029/2007WR006552.

Mishra, U., Mohapatra, A.K., Mandal, A., Singh, A., 2023. Identification of potential artificial groundwater recharge sites in an alluvial setting: a coupled electrical resistivity tomography and sediment characterization study. Groundw. Sustain. Dev. 20, 100875. https://doi.org/10.1016/j.gsd.2022.100875.

Molina-Giraldo, N., Bayer, P., Blum, P., Cirpka, O.A., 2011. Propagation of seasonal temperature signals into an aquifer upon bank infiltration. Ground Water 49, 491–502. https://doi.org/10.1111/j.1745-6584.2010.00745.x.

Mulligan, A.E., Evans, R.L., Lizarralde, D., 2007. The role of paleochannels in groundwater/seawater exchange. J. Hydrol. 335, 313–329. https://doi.org/10.1016/j.jhydrol.2006.11.025.

Munn, J.D., Maldaner, C.H., Coleman, T.I., Parker, B.L., 2020. Measuring fracture flow changes in a bedrock aquifer due to open hole and pumped conditions using active distributed temperature sensing. Water Resour. Res. 56. https://doi.org/10.1029/2020wr027229.

Nikles, M., Thevenaz, L., Robert, P.A., 1997. Brillouin gain spectrum characterization in single-mode optical fibers. J. Lightwave Technol. 15, 1842–1851. https://doi.org/10.1109/50.633570.

Nikles, M., Thévenaz, L., Salina, P., Robert, P.A., 1996. Local analysis of simulated Brillouin interaction in installed fiber optic cables. Presented at the Symposium on Optical Fiber Measurements (OFMC'96), NIST Special Publication 905, Boulder CO, pp. 111–114.

Omnisens, 2019. Vision interrogator Fiber optic distributed temperature and strain analyzer. User manual Vision Interrogator Version 1-10-a – EN-FR.

Palmer, C.D., 1993. Borehole dilution tests in the vicinity of an extraction well. J. Hydrol. 146, 254–266.

Palmieri, L., Schenato, L., Santagiustina, M., Galtarossa, A., 2022. Rayleigh-based distributed optical fiber sensing. Sensors 22, 6811. https://doi.org/10.3390/s22186811.

Perzan, Z., Chapin, T., 2023. WellSTIC: a cost-effective sensor for performing point dilution tests to measure groundwater velocity in shallow aquifers. e2022WR033223 Water Resour. Res. 59. https://doi.org/10.1029/2022WR033223.

Piccinini, L., Fabbri, P., Pola, M., 2016. Point dilution tests to calculate groundwater velocity: an example in a porous aquifer in northeast Italy. Hydrol. Sci. J. 61, 1512–1523. https://doi.org/10.1080/02626667.2015.1036756.

Ravet, F., Zou, L., Bao, X., Chen, L., Huang, R.F., Khoo, H.A., 2006. Detection of buckling in steel pipeline and column by the distributed Brillouin sensor. Opt. Fiber Technol. 12, 305–311. https://doi.org/10.1016/j.yofte.2005.12.002.

Read, T., Bour, O., Bense, V., Le Borgne, T., Goderniaux, P., Klepikova, M.V., Hochreutener, R., Lavenant, N., Boschero, V., 2013. Characterizing groundwater flow and heat transport in fractured rock using fiber-optic distributed temperature sensing. Geophys. Res. Lett. 40, 2055–2059. https://doi.org/10.1002/grl.50397.

Romanet, M., 2024. Réflectométrie Brillouin par comptage de photons pour les capteurs distribués à fibres optiques (Thèse). Université de France-Comté, Besançon.

Romanet, M., Giraldo, L.M., Zerbib, M., Rochat, E., Phan Huy, K., Beugnot, J.-C., 2023. Towards single-photon Brillouin optical time domain reflectometry. Opt. Express 31, 21542. https://doi.org/10.1364/OE.492488.

Sai Louie, A.J., Morgan, L.K., Banks, E.W., Dempsey, D., Wilson, S., 2023. Active-distributed temperature sensing dataset beneath a braided river. Data Brief 51, 109756. https://doi.org/10.1016/j.dib.2023.109756.

Samadder, R.K., Kumar, S., Gupta, R.P., 2011. Paleochannels and their potential for artificial groundwater recharge in the western Ganga plains. J. Hydrol. 400, 154–164. https://doi.org/10.1016/j.jhydrol.2011.01.039.

Saphores, E., Leray, S., Suárez, F., 2024. Groundwater–surface water exchange from temperature time series: a comparative study of heat tracer methods. J. Hydrol. 632, 130955. https://doi.org/10.1016/j.jhydrol.2024.130955.

Schenato, L., 2017. A review of distributed fibre optic sensors for geo-hydrological applications. Appl. Sci. 7, 896. https://doi.org/10.3390/app7090896.

Selker, F., Selker, J., 2018. Investigating water movement within and near wells using active point heating and fiber optic distributed temperature sensing. Sensors 18, 1023. https://doi.org/10.3390/s18041023.

Selker, J.S., Thévenaz, L., Huwald, H., Mallet, A., Luxemburg, W., van de Giesen, N., Stejskal, M., Zeman, J., Westhoff, M., Parlange, M.B., 2006. Distributed fiber-optic temperature sensing for hydrologic systems: rapid communication. Water Resour. Res. 42. https://doi.org/10.1029/2006WR005326.

Shafer, J.M., Brantley, D.T., Waddell, M.G., 2010. Variable-density flow and transport simulation of wellbore brine displacement. Groundwater 48, 122–130. https://doi.org/10.1111/j.1745-6584.2009.00594.x.

Shanafield, M., Banks, E.W., Arkwright, J.W., Hausner, M.B., 2018. Fiber-optic sensing for environmental applications: where we have come from and what is possible. Water Resour. Res. 54, 8552–8557. https://doi.org/10.1029/2018WR022768.

Romanet, M., Labbe, J., Matic, A., Zerbib, M., Amiotte-Suchet, P., Bertrand, X., Karbowiak, T., Phan Huy, K., Celle, H., Beugnot, J.-C., 2026. Distributed Brillouin fiber optic temperature sensing for hydrogeology. Institute of Electrical and Electronic Engineers.

Simon, N., 2020. Développement des méthodes actives de mesures distribuées de température par fibre optique pour la quantification des écoulements souterrains : apports et limites pour la caractérisation des échanges nappe/rivière (Thèse). Université Rennes 1, Rennes.

Simon, N., Bour, O., 2023. An ADTS toolbox for automatically interpreting active distributed temperature sensing measurements. Groundwater 61, 215–223. https://doi.org/10.1111/gwat.13172.

Simon, N., Bour, O., Faucheux, M., Lavenant, N., Le Lay, H., Fovet, O., Thomas, Z., Longuevergne, L., 2022. Combining passive and active distributed temperature sensing measurements to locate and quantify groundwater discharge variability into a headwater stream. Hydrol. Earth Syst. Sci. 26, 1459–1479. https://doi.org/10.5194/hess-26-1459-2022.

Simon, N., Bour, O., Lavenant, N., Porel, G., Nauleau, B., Klepikova, M., 2023. Monitoring groundwater fluxes variations through active-DTS measurements. J. Hydrol. 622, 129755. https://doi.org/10.1016/j.jhydrol.2023.129755.

Simon, N., Bour, O., Lavenant, N., Porel, G., Nauleau, B., Pouladi, B., Longuevergne, L., Crave, A., 2021. Numerical and experimental validation of the applicability of active-DTS experiments to estimate thermal conductivity and groundwater flux in porous media. Water Resour. Res. 57, e2020WR028078. https://doi.org/10.1029/2020WR028078.

Stauffer, F., Bayer, P., Blum, P., Giraldo, N.M., Kinzelbach, W., 2013. Thermal Use of Shallow Groundwater, 0th ed. CRC Press. Doi: 10.1201/b16239.

Thevenaz, L., Nikles, M., Fellay, A., Facchini, M., Robert, P.A., 1998. Applications of distributed Brillouin fiber sensing. In: Rastogi, P.K., Gyimesi, F. (Eds.), Presented at the International Conference on Applied Optical Metrology, Balatonfured, Hungary, pp. 374–381. https://doi.org/10.1117/12.323342.

Tyler, S.W., Selker, J.S., Hausner, M.B., Hatch, C.E., Torgersen, T., Thodal, C.E., Schladow, G.S., 2009. Environmental temperature sensing using Raman spectra DTS fiber-optic methods. Water Resour. Res. W00D23 45, 1–11. https://doi.org/10.1029/2008WR007052.

Ukil, A., Braendle, H., Krippner, P., 2012. Distributed temperature sensing: review of technology and applications. IEEE Sens. J. 12, 885–892. https://doi.org/10.1109/JSEN.2011.2162060.

van de Giesen, N., Steele-Dunne, S.C., Jansen, J., Hoes, O., Hausner, M.B., Tyler, S., Selker, J., 2012. Double-ended calibration of fiber-optic raman spectra distributed temperature sensing data. Sensors 12, 5471–5485. https://doi.org/10.3390/s120505471.

Vogelgesang, J.A., Holt, N., Schilling, K.E., Gannon, M., Tassier-Surine, S., 2020. Using high-resolution electrical resistivity to estimate hydraulic conductivity and improve characterization of alluvial aquifers. J. Hydrol. 580, 123992. https://doi.org/10.1016/j.jhydrol.2019.123992.

Wang, W., Pang, H., Lou, F., Ma, Z., Zhu, B., Ji, S., Chen, Z., Hong, B., 2025. Hybrid GA-ANN-LSSVM algorithm for adaptive Brillouin frequency shift extraction in long-distance oil and gas pipeline monitoring. Opt. Express 33, 24429. https://doi.org/10.1364/OE.561846.

Wildemeersch, S., Jamin, P., Orban, P., Hermans, T., Klepikova, M., Nguyen, F., Brouyère, S., Dassargues, A., 2014. Coupling heat and chemical tracer experiments for estimating heat transfer parameters in shallow alluvial aquifers. J. Contam. Hydrol. 169, 90–99. https://doi.org/10.1016/j.jconhyd.2014.08.001.

Williams, A., Bloomfield, J., Griffiths, K., Butler, A., 2006. Characterising the vertical variations in hydraulic conductivity within the Chalk aquifer. J. Hydrol. 330, 53–62. https://doi.org/10.1016/j.jhydrol.2006.04.036.

Yin, M., Ma, R., Zhang, Y., Lin, J., Guo, Z., Zheng, C., 2023. Competitive control of multiscale aquifer heterogeneity on solute transport in an alluvial aquifer. J. Hydrol. 616, 128819. https://doi.org/10.1016/j.jhydrol.2022.128819.